Published online 10 November 2010 *Nucleic Acids Research, 2011, Vol. 39, No. 5* ***1919–1932***
doi:10.1093/nar/gkq1044

Sequence-dependent cooperative binding of p53 to DNA targets and its relationship to the structural properties of the DNA targets

Itai Beno, Karin Rosenthal, Michael Levitine, Lihi Shaulov and Tali E. Haran*

Department of Biology, Technion, Technion City, Haifa 32000, Israel

Received August 9, 2010; Revised September 20, 2010; Accepted October 12, 2010

ABSTRACT

The prime mechanism by which p53 acts as a tumor suppressor is as a transcription factor regulating the expression of diverse downstream genes. The DNA-binding domain of p53 (p53DBD) interacts with defined DNA sites and is the main target for mutations in human primary tumors. Here, we show that the CWWG motif, found in the center of each consensus p53 half-site, is a key player in p53/DNA interactions. Gel-mobility-shift assays provide a unique opportunity to directly observe the various oligomeric complexes formed between p53DBD and its target sites. We demonstrate that p53DBD binds to p53 consensus sites containing CATG with relatively low cooperativity, as both dimers and tetramers, and with even lower cooperativity to such sites containing spacer sequences. p53DBD binds to sites containing CAAG and CTAG with measurable affinity only when imbedded in two contiguous p53 half-sites and only as tetramers (with very high cooperativity). There are three orders-of-magnitude difference in the cooperativity of interaction between sites differing in their non-contacted step, and further two orders-of-magnitude difference as a function of spacer sequences. By experimentally measuring the global structural properties of these sites, by cyclization kinetics of DNA minicircles, we correlate these differences with the torsional flexibility of the binding sites.

INTRODUCTION

The tumor suppressor protein p53 is a transcription factor (TF) that in response to various types of cellular stress regulates the expression of a variety of genes involved in cell-cycle control, apoptosis, DNA repair and cell differentiation (1–3), by binding sequence-specifically to defined DNA targets (4,5). Abrogation of p53 sequence-dependent binding is implicated in ~50% of all known cancers (1,2). Recently, p53 was shown to have additional roles in senescence, development and the immune system, unrelated to cancer surveillance (6,7). The complexity of p53 functions is mirrored in the complexity of its structure and binding mechanism. p53 molecules consist of four major functional domains (8). The N-terminus contains a transactivation domain (TA); the core domain (CD) contains the sequence-specific DNA-binding domain (DBD); and the C-terminal domain includes a tetramerization domain and a regulatory domain that contain a separate sequence non-specific DNA-binding activity (9). The core domain of p53 contains 95% of the missense mutations identified in human tumors (10). This highlights the importance of sequence-specific p53/DNA interactions for p53 functions. The consensus binding site defined *in vitro* consists of two decameric sequences, or half-sites, with the general form RRRCWWGYYY (R = A,G;W = A,T;Y = C,T), separated by 0–13 bp (4). However, *in vivo* defined binding sites contain fewer spacer sequences (5,11).

We have recently shown that changes in both direct and indirect readout of p53 DNA-binding sites (or response elements, REs) play a central role in modulating the DNA binding affinity of p53DBD (12). In the crystal structure determination of functional complexes of p53DBD and three different DNA sequences, the protein–DNA interface varies as a function of the DNA base sequence (12). DNA-binding measurements show a correlation between binding affinities of the complexes and the protein–DNA interface geometries, and that the complexes varies in both direct-readout effects (changes in protein–DNA contacts) and indirect-readout effects (changes in DNA structure). The crystal structures of p53DBD/DNA complexes (12,13) showed that the middle WW dinucleotide (also called base-pair step or doublet) in each half-site is not directly contacted in the

*To whom correspondence should be addressed. Tel: +972 4 8293767; Fax: +972 4 8225153; Email: bitali@tx.technion.ac.il

complex with p53DBD. Nonetheless, this position is highly conserved in natural p53 REs, with a marked preference for A–T and A–A, but not T–A base–pair steps (14–16).

The level of DNA binding (17) and transcriptional activation (14,18) vary significantly among p53-regulated genes, due to variations within the individual response elements, their internal arrangement, number of decameric repeats and location with respect to the start site (14,18). Moreover, alteration in the non-contacted WW step causes significant changes in transactivation activity, with A-T containing sequences being those with significantly higher activity (18,19). p53 was recently shown to be functional also from sequences that have only one canonical half-site (20). Transactivation from these sites was shown to be sequence-dependent and to operate through the binding of p53 tetramers (20).

It is well established that the functional unit of p53 binding to DNA is a tetramer and that the binding of p53 to its specific REs is highly cooperative (21–24). p53DBD is monomeric in solution, whereas constructs containing the tetramerization domain are mostly dimeric in solution. Thus, tetramerization is mediated by specific binding of p53 to its REs (24). The ability to dimerize is encoded within p53DBD (12,25–28) and is located in the H1 helix, the Zn cluster, and in regions of the L2 and L3 loops from each CD. This intradimer protein–protein interface, or symmetrical interface (12), is stabilized by various salt bridges, hydrophobic interactions and water-mediated polar interactions (12). The other protein–protein interface observed in p53 tetramers is the translational interface that forms between dimers (12). We show here that p53 binding cooperativity is encoded in the DNA sequence of p53 binding sites, and that it spans five orders of magnitude as a function of DNA sequence. The key to the differential changes in cooperative binding is the torsional flexibility of the central CWWG motif of p53 binding sites, as determined from cyclization kinetics experiments.

MATERIALS AND METHODS

Protein and DNA

Human p53 core domain (residues 94–293, referred to as p53DBD) and a p53 construct containing the N-terminus as well (p53TD, amino acids 1–290) were a kind gift from Zippora Shakked (Weizmann Institute of Science). The cloning, transformation, overexpression and purification are as described by Kitayner *et al*. (12). Protein concentration was determined spectroscopically, using an estimated extinction coefficient of 17 420 and 33 920 $M^{-1}\,cm^{-1}$, as calculated by the ProtParam tool of the ExPASy server (29) for the p53DBD and p53TD constructs, respectively. Prior to the binding studies, the fraction of p53DBD molecules active for DNA binding was determined as described previously (30). All DNA sequences for the electrophoretic mobility shift assay (EMSA, shown in Table 1) were synthesized by Sigma Genosys (Israel) and purified by a reverse-phase cartridge. The sequences for the EMSA experiments were designed as intramolecular hairpin constructs, with between 23 and 27 bp in the stem, and with five cytosines in the loop as previously described (12,30). Con3 sequence was also synthesized as an intramolecular dumbbell construct (Table 1), with two hairpin loops each containing five cytosines (31). The DNA test sequences for cyclization experiments [bottom polymerase chain reaction (PCR) templates] were synthesized by Sigma Genosys (Israel), and contained three copies of the decameric half-site of Con1, Con2, Con3, Con4, Con5 or con6 (Table 2), whereas the library DNA sequences (top PCR templates) and the fluorescein- and tetramethylrhodamine (TAMRA)-labeled oligonucleotide primers (32) were synthesized by the Keck Foundation Laboratory at Yale University, and purified as previously described (32).

Binding stoichiometry measurements

The experiments were carried out by the continuous variation (Job plot) method (33). In this assay, the total molar

Table 1. Binding affinity and cooperativity of p53DBD interaction with the p53 REs studied here

Name	Sequence	$k_1 = k_2 =$ dimer K_d[a]	$K_{a2} = k_1k_2k_{12} =$ tetramer K_d (M^2)[a]	Dimer equiv tetramer K_d[a,b]	$k12$[a]
Con1	C**GGGCA**TGTCC**GGGCA**TGTCCTG	314 (14) nM	1.0 (0.2) E-14	64 (4) nM	25 (2)
Con1 HS	TGGTTGC**GGGCA**TGTCCTGGGTA	305 (24) nM	–	–	–
Con1 and 2-bp spacer	C**GGGCA**TGTCCgc**GGGCA**TGTCCTG	442 (20) nM	3.9 (0.4) E-13	435 (32) nM	1.1 (0.2)
Con1 and 4-bp spacer	C**GGGCA**TGTCCtgct**GGGCA**TGTCCTG	581 (46) nM	2.1 (0.2) E-12	1.02 (0.06) μM	0.34 (0.06)
Con2	C**GGGCT**AGTCC**GGGCT**AGTCCTG	~25 (5) μM[c]	1.0 (0.3) E-13	252 (19) nM	~10 000 (3000)
Con2 HS	TGGTTGC**GGGCT**AGTCCTGGGTA	3.6 (0.4) μM	–	–	–
Con2 and 2-bp spacer	C**GGGCT**AGTCCgc**GGGCT**AGTCCTG	2.8 (0.3) μM	2 (1) E-11	3 (0.8) μM	0.9 (0.2)
Con2 and 4-bp spacer	C**GGGCT**AGTCCtgct**GGGCT**AGTCCTG	9 (2) μM	2.8 (0.6) E-10	11 (2) μM	0.6 (0.1)
Con3	C**GGGCA**AGTCC**GGGCA**AGTCCTG	~11 (1) μM[c]	1.1 (0.1) E-13	227 (14) nM	~2500 (500)
Con3 nicked dumbbell	CGGCGG**C****GGGCA**@AGTCC**GGGCA**AGTCCTG[d]	600 (100) nM[e]	1.1 (0.2) E-12	–	9.0 (0.6)

[a]The values are average of four to eight independent experiments conducted with each sequence; the values in parenthesis are the standard error of the mean.
[b]Since the half-sites are identical ($k_1 = k_2$) one can take the square root of the expression for K_{a2} and determine the 'dimer equivalent tetramer K_d',
[c]K_d estimated by inserting zeros to account for the unobserved dimer bands (see text for details).
[d]@ = nick in sequence. Double strands are held by two hairpin loops, i.e. a dumbbell. All other sequences contain a single hairpin loop at the 3′ end.
[e]Value for dimer binding to the nicked half-site; the value for the other half site is that of the half site of Con3 (see text for details).

Table 2. Best-fit parameters for p53 REs from analysis by cyclization kinetics

Name	sequence	Bend angle (°)[a,b]	Twist angle (°)[b]	Roll and tilt fluctuations (°)[b]	Twist fluctuations (°)[b]	Torsional force constant × 10^{19} erg•cm
con1	GGGCATGTCC	0.47 (0.09)	34.13 (0.11)	4.49 (0.10)	5.62 (0.09)	1.432
con2	GGGCTAGTCC	0.48 (0.07)	34.15 (0.10)	4.45 (0.08)	4.65 (0.07)	2.094
con3	GGGCAAGTCC	0.21 (0.08)	34.17 (0.10)	4.45 (0.10)	4.71 (0.07)	2.044
con4 (GGG)	GGGCATGCCC	0.80 (0.09)	34.18 (0.11)	4.45 (0.10)	5.70 (0.09)	1.395
con5 (GGA)	GGACATGTCC	0.85 (0.07)	34.22 (0.08)	4.51 (0.07)	5.21 (0.08)	1.671
con6 (AGG)	AGGCATGCCT	0.45 (0.10)	34.16 (0.10)	4.43 (0.10)	5.47 (0.09)	1.514
B-DNA[c]		0.61 (0.09)	34.22 (0.09)	4.50 (0.10)	5.06 (0.09)	1.771

All measurements were made at 21°C.
[a]Bending is by roll and its center is located at the fourth step of all sequences, i.e. at the C-A or C-T step.
[b]Numbers in parenthesis are the simulation errors, calculated as described in ref. (40).
[c]From Zhang *et al.* (32).

concentration (protein and DNA) was fixed at 600, 900 or 1200 nM, and the protein mole fraction was varied regularly from 0 to 0.983 (0 to 590, 890 or 1180 nM, respectively). Other reaction conditions are as described below for the binding affinity measurements. In addition, binding stoichiometry measurements were also carried out by mixing of two different p53 constructs (p53DBD and p53TD). This assay was carried out as described below for the binding affinity measurements, except that protein concentration was an equimolar mixture of the two proteins used in these experiments, and the EMSA gels were 4% (37.5:1 acrylamide:bisacrylamide ratio).

Binding affinity measurements

Radiolabeled and gel-purified hairpin duplexes (<0.1 nM) and increasing amounts of p53DBD were incubated on ice for 2 h in a buffer containing 50 mM Tris–HCl (pH 7.5), 10 mM MgCl2, 1 mM ATP, 25 U/ml BSA, 10% glycerol, 10 mM DTT and 200 mM KCl. Complexes were resolved from free DNA by electrophoresis on native gels (6%, 37.5:1 acrylamide: bisacrylamide ratio). The gels were run at 550 V and 4°C in a running buffer containing 1 × TG [25 mM Tris–HCl (pH 8.3), 190 mM glycine], until the bromophenol blue dye migrated 8 cm.

Dried gels were quantified using a Fujii FLA 5000 phosphoimager. We have analyzed the system separately for each bound band using TotalLab v2 (Nonlinear Dynamics Ltd., UK). Boxes were defined surrounding each band on the gel, such that each box covered only the main band, and did not include any gel-instability smear extending forward on the gel. The sizes of the boxes were defined by the profile option of TotalLab and not by visual inspection of the gels. Overall background was subtracted from the entire gel in TotalLab by defining a box in the surrounding gel area that produced a base line that passes at the bottom edge of the bands peaks. In addition, we subtracted a local background, only from the bound bands, such that the region above the free DNA band, on the lane in which no protein was added, was equal to exactly 0.00 unit of photostimulated luminescence (PSL) from the photostimulable phosphor image plate, to account for possible trail of radioactivity left by the migration of the free DNA ahead of the bound complexes (34). Θ_i, the fraction of DNA molecules with i protein molecules bound, was calculated from the equation: $\Theta_i = (\text{PSL-bg})_i / \Sigma_i(\text{PSL-bg})_i$ where bg is the background, and the summation is over all the bands in a given lane.

Association binding constants were calculated using nonlinear least-squares methods of parameter estimation (SigmaPlot, Jandel Scientific, CA, USA). Since the stoichiometry measurements have shown that the apparent binding unit is a dimer of p53DBD (see 'Results' section), we used a regular two binding site model for all target sites used in this study, except those that harbor only one half-site (Con1HS and Con2HS), where we used a regular one site model (35–37). For gel patterns showing only the tetramer binding species, we added zeros to account for the unobserved dimer bands. Thus, the following equations were used:

$$\Theta_0 = 1/(1+K_{a1} * [P]+K_{a2} * [P]^2) \quad (1)$$

$$\Theta_1 = K_{a1}*[P]/(1+K_{a1}*[P]+K_{a2}*[P]^2) \quad (2)$$

$$\Theta_2 = K_{a2}*[P]^2/(1+K_{a1}*[P]+K_{a2}*[P]^2) \quad (3)$$

Where P is the protein and the macroscopic association binding constants are K_{a1} and K_{a2}, for the dimeric and the tetrameric species, respectively. Since in all target sites (except nicked Con3) the two half-sites are identical, it is possible to calculate intrinsic microscopic binding constants and an explicit cooperativity constant (37) as follows:

$$K_{a1} = k_1+k_2 = 2k_i \quad (4)$$

$$K_{a2} = k_1k_2k_{12} = k_i^2k_{12} \quad (5)$$

where k_1, and k_2 are the intrinsic microscopic binding constants for each half-site and k_{12} is the cooperativity constant (37). k_{12} measures the increase (or decrease) in the binding affinity of the second dimer relative to that of the first dimer due to the cooperativity of the binding interaction. For targets with identical half-sites, and assuming equipartition of binding free energies, an apparent dimer-equivalent association constant can be calculated by taking the square root of the K_{a2} value. The reported values (Table 1) are the dissociation binding constants, which are the reciprocal of the

association binding constants. The values in parenthesis in the tables, in figure legends and in the text are the standard error of the mean (SEM). The error bars in the graphs are standard deviation (SD).

Preparation of DNA constructs for cyclization experiments

Constructs were synthesized using the PCR scheme developed by Zhang and Crothers (32). PCR was carried out using the PCR-Ready High Yield clear kit (Syntezza Bioscience Ltd, Israel), supplemented with 100 ng of each top and bottom DNA templates, and 0.5 μM of each primer in a final volume of 50 μl. The PCR had two stages. In the first stage, a double-stranded intermediate was formed from the top and bottom templates by extension from the 10 bp overlap between the templates (32). This was done by subjecting the PCR tubes to 2 min at 94°C, 2 min at 30°C, then increase to 68°C by 2°C increments/45 s and finally 72°C for 60 s. The second stage consisted of 31 cycles of 45 s at 94°C, 59°C and 72°C, which was terminated with 72°C for 15 min. PCR products were purified using Sephadex G-25 (Sigma-Alderich) columns, digested with 15 units of ClaI enzyme in 60 μl for 1–3 h, and then purified on 10% (37.5:1 acrylamide:bis) native gel (40 cm long) in the dark. DNA bands were cut out from the gel under ultraviolet (UV) illumination after 15 min staining with SYBR gold solution (Molecular Probes). Gel pieces were electroeluted and concentrated using millipore Centricon (Ultracell YM-30) and Centrilutor Micro-Electroeluter (Millipore). Residual SYBR gold was removed from the stained DNA by EtOH precipitation.

Cyclization kinetics and simulation of cyclization data

Cyclization kinetics measurements were carried out as described previously (32), using similar instrumentation. DNA concentration was 0.5–2 nM, which yielded initial emission readings of 70–250 arbitrary units. Initially, each DNA construct was measured in several ligase concentrations, to make sure that measurements are carried out in the linear range of ligase concentrations (32). Final ligase concentration used were 1 kU/ml for constructs 156L14 (the in-phase construct for all test sequences) and 156L16 of the phasing assay of all test sequences, and constructs 154–160L14 of the total-length assay; 2 kU/ml was used for all other constructs. The probability of ring closure of DNA molecules, or the *J*-factor, is defined (38) as the ratio of the cyclization equilibrium constant to the bimolecular equilibrium constant for joining two molecules ($J = K_c/K_a$), and it has been shown (39) to be equal (under certain conditions) to the ratio of the corresponding rate constants ($J = k_1/k_2$). k_2 is the same for all constructs with the same cohesive ends, and all measurements were done relative to a B-DNA test sequence whose *J*-factor is known (32). From measurements of the rate of cyclization of this construct ($k_1^{\text{B-DNA}}$) and its known *J*-factor, the *J*-factor of each test sequence was determined by $J_{\text{test}} = J_{\text{B-DNA}} * k_1^{\text{test}} / k_1^{\text{B-DNA}}$, for each specific ligase concentration.

Quantitative data on the conformational properties of the tested DNA molecules were derived by computer modeling of the experimental *J*-factors, based on a model for the structural properties of the tested DNA molecules. Simulation of the cyclization data was carried out using the new theory developed by Zhang and Crothers (40). The program we got was written for the optimization of two structural parameters, and it was extended by us to the simultaneous minimization of the error between simulation and experimental values of four structural parameters: bend angle, helical twist angle, bend flexibility and torsional flexibility. Sixteen *J*-factors were used for each simulation (five for the phasing assay and 11 for the total-length assay).

Statistical analysis of validated p53 REs

The dispersion of averaged structural parameters from their values in protein–DNA complexes (41), measured by the standard deviation, was taken as a measure of the flexibilities of individual DNA base-pair steps. All currently available p53 REs (42) with decameric half-sites that contain a CNNG motif at their center (241 half-sites) were included in the analysis. For each sequence, we calculated the mean and variance of the twist, slide and roll dispersion along the entire half-site. We then grouped these sequences by the identity of the NN step of the central CNNG motif and calculated the mean and the variance of these parameters for each group. We calculated a two-sample *t*-statistic to assess the significance of the difference between groups, by calculating the ratio of the difference between the mean values to the standard error of the difference between the means, separately for each structural parameter. The distributions of the *t* statistic were approximated to a *t*-distribution by using the exact method to calculate the degrees of freedom from the data (43). Since the degrees of freedom, as calculated by this method, depend on the variance of the calculated parameter, they are different for each structural parameter.

RESULTS AND DISCUSSION

Binding of p53DBD to p53 sites as a function of the CWWG motif

The CWWG region is the most conserved region of p53 REs (44), even though the WW dinucleotide is uncontacted in complex with p53DBD (12,13). To probe the role of the non-contacted central dinucleotide in p53/DNA interactions, we studied the effect of changing the central step on p53DBD binding affinity to these targets. We started with the sequence GGGCATGTCC (Con1, Table 1), because it is based on a decamer sequence that was identified by *in vitro* selection experiments as a strong p53-binding site (5), with high transactivation activity *in vivo* (18). We then changed the middle dinucleotide within each half-site to T–A (Con2, Table 1) or A–A (Con3, Table 1). The results of EMSAs with these sequences are shown in Figure 1. Surprisingly, a major variability in this series was the stoichiometry of the binding interaction, i.e. the oligomeric state of p53DBD in the

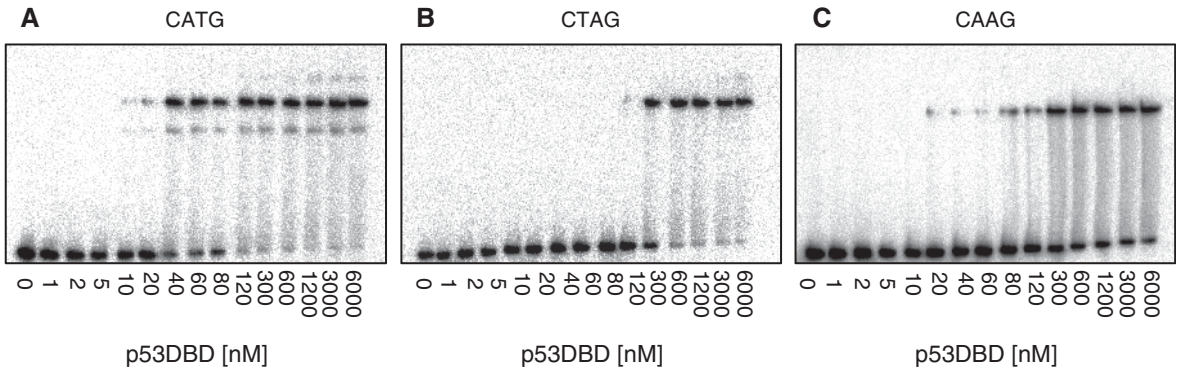

Figure 1. Binding affinity measurements by EMSA of p53 consensus REs as a function of the central CWWG motif. (**A**) Con1, with a central CATG motif. (**B**) Con2, with CTAG. (**C**) Con3, with CAAG. DNA targets were imbedded in hairpin constructs (concentration <0.1 nM). Upper bands show protein bound DNA and lower bands show unbound DNA. The number below each gel is the concentration of p53DBD monomers active for DNA binding. The gels are representative examples of four to eight independent experiments conducted with each sequence.

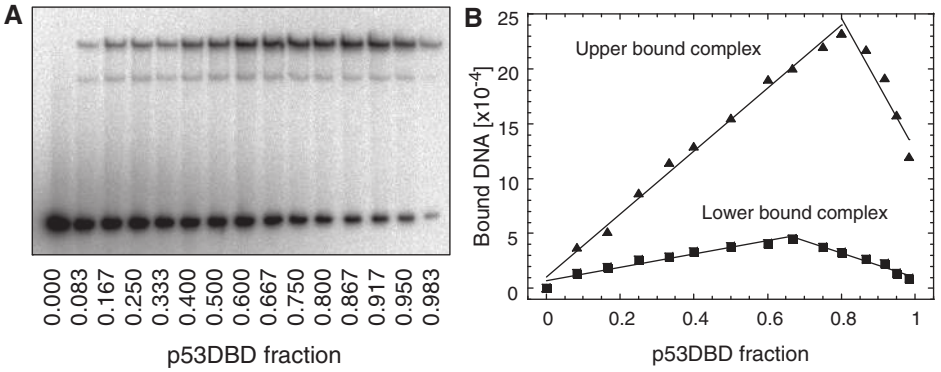

Figure 2. Continuous variation analysis of p53DBD binding to Con1. (**A**) A representative EMSA gel of p53DBD binding to Con1 (of three independent experiments). Total macromolecular concentration was fixed at 600 nM. The mole fraction of protein, shown below the gel, increased across the gel. (**B**) Analysis by a Job plot of the data from (A). The lines are the least-square fits to the rising and falling subsets of the data. Their intersection yields a binding stoichiometry of 1:3.94 (0.06) for the upper bound complex and 1:1.94 (0.08) for the lower bound complex.

complexes formed with each target. Con1 showed two distinct shifted bands, a dominant upper band and a minor lower band, similar to those displayed by the sequences studied by Kitayner *et al*. (12), whereas Con2 and Con3 show only the major upper band. Gel-mobility-shift assays are unique in their ability to distinguish between complexes that differ in their oligomeric composition (37,45,46).

To quantify these gels with confidence, and for each species separately, we must first determine the exact binding stoichiometry of each complex in the gel. The stoichiometry was determined using the continuous variation (Job plot) assay (33). In this method, the total molar concentration of protein and DNA is held constant, whereas their molar ratios are continuously varied, from only DNA to almost only protein (Figure 2A). The ratio at which the bound complex is maximal is the binding stoichiometry for that complex. The reaction was carried out using the Con1 sequence with the total molar concentration fixed at 600 nM, which is thus significantly above the dissociation constant of the complex (Table 1). Approximating the experimental points by two lines of limiting slopes (Figure 2B) produced a stoichiometry of 1:3.94 (0.06) for the upper bound complex and 1:1.94 (0.08) for the lower bound complex, which established that the upper bound complex is a tetramer of p53DBD and the lower one is a dimer of p53DBD bound to DNA. A proof for cooperative binding is when the maximum in the Job plot (and hence the resultant stoichiometry) is independent of the total protein and DNA concentration (33). Hence, we repeated the experiment at 900 nM and at 1200 nM total molar concentration (Supplementary Figure S1). The resulting stoichiometry was 1:4.0 (0.2) and 1:1.96 (0.07) at 900 nM, and 1:4.1 (0.2) and 1:2.1 (0.2) at 1200 nM, for the upper and the lower bound bands, respectively, thus establishing that p53DBD binds cooperatively to its REs, whether the binding is as a tetramer (upper bound band) or as a dimeric species (lower bound band).

Another convenient method to easily check the binding stoichiometry is to mix together two proteins constructs differing only in their molecular weight (47). Therefore, to further elucidate the nature of the different binding species we ran an EMSA gel with the Con1 target, using an equimolar mixture of two different p53 constructs: p53DBD (amino acids 94–293) and p53TD (amino acids 1–290). Supplementary Figure S2A shows that p53TD formed a complex with Con1 that migrates higher on the gel than the complex containing p53DBD, and that only a

single complex band is observed. Supplementary Figure S2B shows that upon mixing the two proteins, the upper band is split into three separate bands, of which the lower one is the prominent one. This confirmed that the uppermost shifted band with Con1 and p53DBD is a tetramer, and that this tetramer is composed of tightly held dimers. Mixing of independent monomeric species would have resulted in a split to five individual bands. It also confirmed that the lower shifted band with Con1 and p53DBD is not a tetramer. The N-terminal domain is known to have an inhibitory effect on the binding of the DBD to p53 targets (48), which may be the reason why p53TD is not stably bound as a dimer. This is also evident by the lower binding affinity of p53TD to Con1, as manifested by split bands getting weaker as we go up in the gel pattern with the combined proteins.

The gel pattern with the Con1 target, and specifically the dimeric complex, is not a result of complex instability during the electrophoretic run. This can be determined from a time course of the reaction with the Con1 target, where we incubated this target with p53DBD in the regular conditions and loaded equal aliquots of the reaction at 10-min intervals. Supplementary Figure S3 shows that there is no accumulation of the dimeric species as a function of gel run time; on the contrary, the dimeric species became depleted as the complex migrated on the gel, due to gel instabilities. At the second shortest run time (from the right-hand-side of the gel), the dimeric species is 19 (1)% of the total of the two bound bands, whereas at the longest run time it is 14 (2)% of the total.

Changes in the CWWG motif leads to three orders-of-magnitude differences in the degree of cooperative binding

We have quantified the binding affinity in this study separately for each bound band using a two binding site model, shown for Con1, Con2 and Con3 in Figure 3A–C. Such analysis assumes that the minimal binding unit for p53DBD is apparently a dimer. It is known that in solution p53DBD is monomeric (24). However, the binding cooperativity for the monomer–dimer transition is faster than can be observed using these methods. More elaborate models, such as a four binding site model, resulted in significant worse fit between the experimental points and those of the model (data not shown). Since in gels with the Con2 and Con3 targets no bands of dimeric complexes were observed, we have included them in the analysis as having zero occupancy. This led to a significant improvement in the fit of the experimental data over that of using a one-site model (tetramer only), or using a two-site model without dimer occupancy included. However, analysis by two equations that do not include a term for K_{a1} (dimer binding) resulted in the same tetramer K_d.

The results of this analysis (Table 1) showed significant changes between the targets in both the binding affinity and especially in the binding cooperativity. Con1 sequence showed the highest tetramer binding affinity in this series [64 (4) nM] and the lowest binding cooperativity [k_{12} = 25 (2), see 'Material and Methods' section for explanation on analysis method]. Con2 showed the lowest tetramer binding affinity [252 (19) nM] and the highest binding cooperativity (k_{12} ~10 000), and Con3 showed values between these two extremes [tetramer K_d = 227 (14) nM, and k_{12} ~2500]. There is a 4-fold difference in binding affinity between the sites, and a 400-fold difference in the binding cooperativity. The binding affinity of p53DBD dimer to Con1 is 314 (14) nM. Cooperativity constants above ~1000 are not resolvable on EMSA gels (37). They are indeed not observed in the gels of Con2 and Con3 and hence we added them in the analysis with zero occupancy in order to calculate the dimer binding affinity and cooperativity for these sites. The k_{12} values for Con2 and Con3 may therefore be only a rough estimate. However, the difference in k_{12} values among these sites, and between them and that of the Con1 target, is so large that it allows us to conclude that the changes in binding cooperativity between the sites are highly significant.

In all analyzed sequences, we observed a slight systematic underestimation of the bound bands, and a slight systematic overestimation of the free DNA bands, which is due to gel instabilities, at the 3–5 highest protein concentration. When there is only one bound species in the gel experiment (49,50), or when we analyze the bound species together for overall affinity (12), one can extend the bound complexes bands downwards to include such instabilities. However, here there is more than one bound species in the complex with Con1, and hence we delimited the boxes defining the bound complexes tightly around each band. This may also account for the difference in binding affinity of Con1 versus those studied by Kitayner *et al.* (12), where we performed an overall analysis, with boxes extended to the free DNA. Analysis for overall K_d of the Con1 target led to a binding affinity of 20 (2) nM, similar to that of the GGG target of Kitayner *et al.* (12). However, only an analysis for separate binding of each species can demonstrate the vast differences in binding cooperativity between binding sites observed here. EMSA methods, carried out as described in this study, are known to yield robust and precise quantitative results (45,46,51–53). Moreover, EMSA has been shown to be useful also for accurate quantitative determination of cooperativity in protein–DNA interactions, when analyzed as described by Senear and Brenowitz (37), even when the analyzed gels are noisy.

Structural characterization of p53 sites as a function of the non-contacted step

There are many known instances in which DNA is deformed in protein–DNA complexes (54,55). Hence, the different strength of binding and especially binding cooperativity may be due to different deformabilities of the studied targets (56), especially as the targets differ in a region that is uncontacted by the protein in the protein/DNA complex. To address this issue we have measured the global structure and mechanical properties of decamers of Con1, Con2 and Con3 half-sites using the high-throughput DNA cyclization approach developed by Zhang and Crothers (32). In this method, one measures the *J*-factors of a series of DNA molecules, all containing the same test sequence (see 'Materials and Methods' section for details). The relationship between

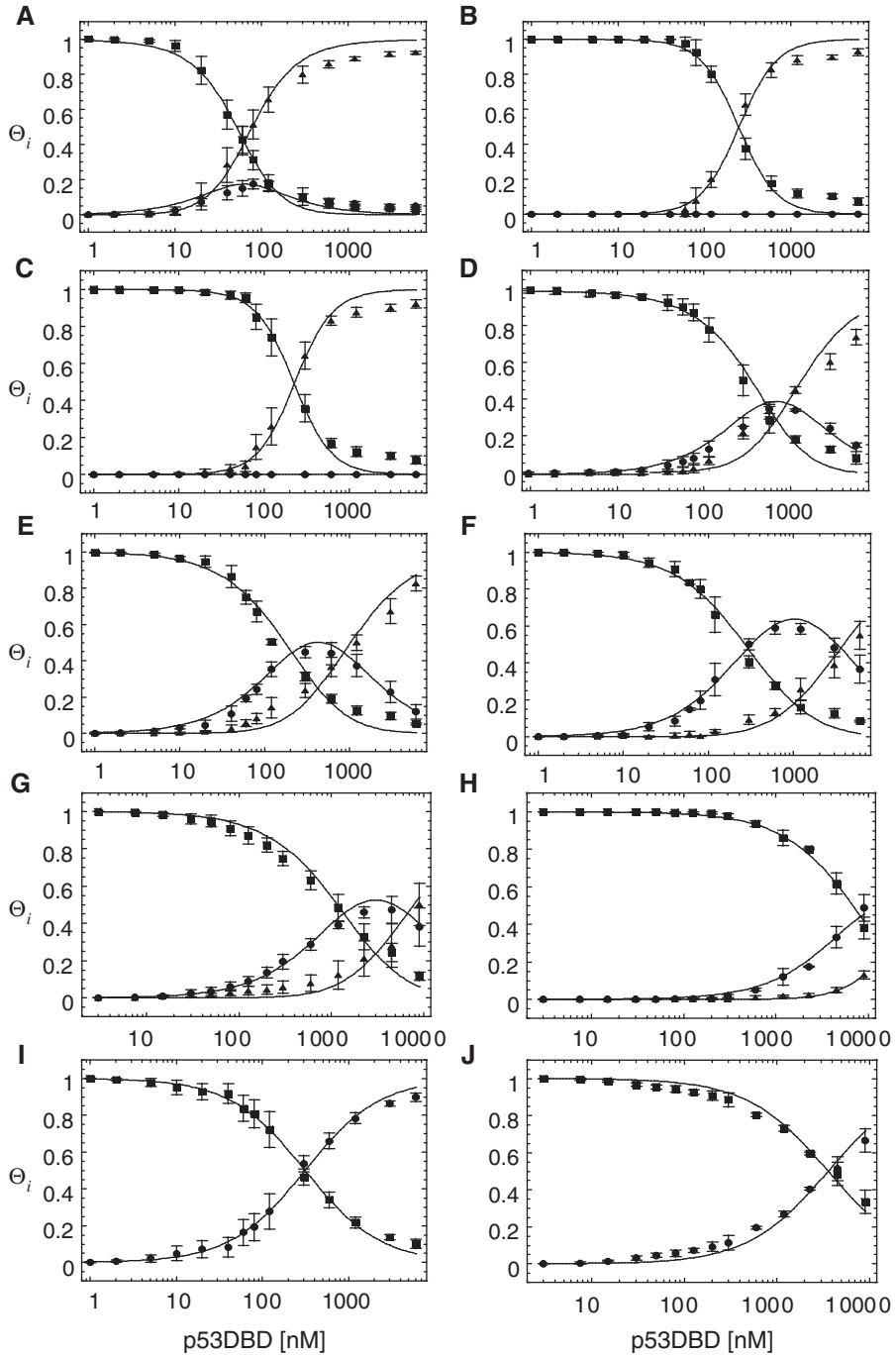

Figure 3. Determination of the relative affinities of p53DBD for binding to the DNA targets studied here. (**A**) Con1. (**B**) Con2. (**C**) Con3. (**D**) Nicked Con3. (**E**) Con1 and 2 bp. (**F**) Con1 and 4 bp. (**G**) Con2 and 2 bp. (**H**) Con2 and 4 bp. (**I**) Con1HS. (**J**) Con2HS. The fraction of DNA molecules with *i* p53DBD molecules bound as a function of the concentration of p53DBD monomers is shown here. DNA concentration is <0.1 nM. Binding was analyzed by a two-site model for all targets except con1HS and con2HS were a one site model was used (solid lines). Squares, unliganded DNA; circles, DNA with one bound dimer; triangles, DNA with two bound dimers (tetramers). The error bars are the SD from four to eight independent experiments conducted with each sequence.

the experimental data and DNA structure is obtained by computer analysis, based on a model for the structural properties of the tested sequences. Specifically, two assays were performed – the phasing assay and the total-length assay (32). In the first assay, the total-length is constant and the phasing between the test sequence and sequences containing curved DNA (A-tracts) is varied. Once the in-phase construct is determined, one varies the total length of the constructs, preserving the relative orientation of the two regions. The phasing assay is sensitive to DNA curvature and bending flexibility. The total-length assay is sensitive to DNA helical repeat and to bending and twist flexibility. Overall, 16 DNA constructs are used to determine four structural parameters for each sequence

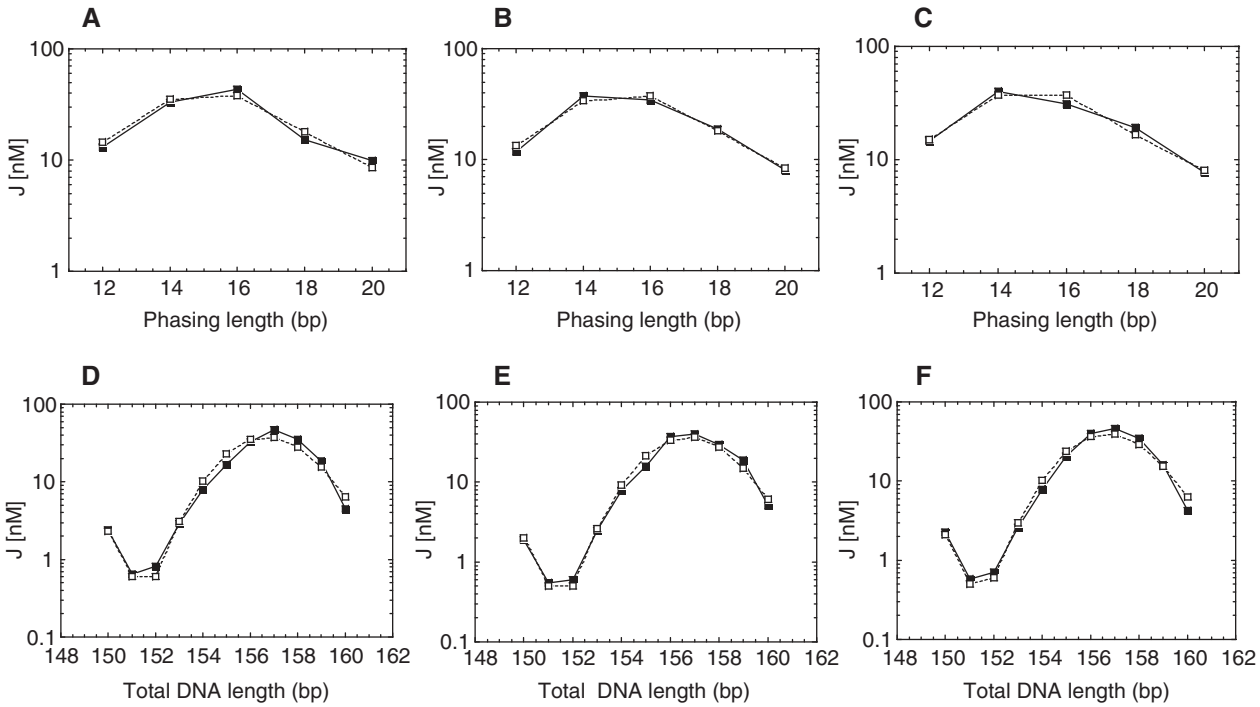

Figure 4. Cyclization kinetics of p53 REs as a function of the central CWWG motif. The *J*-factors for the DNA constructs as a function of either the phasing length (**A–C**), or the total DNA length (**D–F**), for Con1 (A and D), Con2 (B and E) and Con3 (C and F) are shown here. In each case, the test sequence was three repeats of the decameric half site. The solid lines are the experimental curves and the dashed lines are the curves from simulating the data.

(twist angle, bend angle, torsional flexibility and bending flexibility).

Figure 4 shows the results of the phasing and total-length assays for Con1 to Con3. From the final structural parameters (Table 2), it can be observed that the significant difference between these sequences is only in their torsional flexibility. The Con1 decamer is one of the most torsionally flexible sequences determined to date, with 5.62 (0.09)° in twist fluctuations, which result in a torsional force constant of 1.432×10^{-19} erg•cm. Relative to the torsional flexibility of generic B-DNA measured by us [5.06 (0.06)°, Table 2], both Con2 as well as Con3 half-sites are more torsionally rigid [4.64 (0.07)° and 4.71 (0.07)°, respectively]. To understand whether Con1 is unique in being torsionally flexible, we determined by cyclization kinetics the structural properties of three additional p53 consensus binding sites: GGG (also called Con4), GGA (Con5) and AGG (Con6), studied by Kitayner *et al.* (12). Supplementary Figure S4 shows the results of the phasing and total-length assay for these sequences. The final structural values (Table 2) showed that all decamers with a CATG center are more torsionally flexible than sequences with a CAAG or CTAG center. The torsional force constant varies with the inverse square of the rms fluctuation angle. Looking at the values for the torsional force constant (Table 2) we note that the Con4 target (1.395×10^{-19} erg•cm) is ~50% more flexible than either Con2 or Con3 (2.094 and 2.044×10^{-19} erg•cm, respectively). The twist flexibility of the most torsionally rigid DNA molecule, measured so far by cyclization kinetics, is 3.9 (0.3)° (56), which amount to a force constant of 2.98×10^{-19} erg•cm. Thus, the whole range of sequence-dependent twist flexibility is ~2-fold. Previously estimation of the range of sequence-dependent torsional flexibility ranged from nonexistent (57) to around 2-fold (58). Thus, it seems that the ~2-fold range observed in DNA sequences studied so far by cyclization kinetics is about the entire range. Hence, the difference in the torsional force constant between p53 binding sites studied here is significant.

The high torsional flexibility of all CATG decamers is due to the combined flexibilities of the C-A (T-G) steps and not to that of the central A-T step. Using dimeric steps taken from B-DNA crystal structures (59) or DNA structure in protein–DNA complexes (41), Olson and co-workers note that these steps are the most torsionally flexible of all dinucleotide combinations, as inferred from the large dispersion values of these steps around their averaged values.

CTAG containing sequences were proposed to be exceptionally flexible (60), on account of the known flexibility properties of T-A steps (61,62). T-A steps are indeed anisotropically flexible, but their structure is also very context dependent, and thus sequences harboring T-A steps are not well represented by nearest-neighbor models (50). We showed here that within the sequence context of the Con2 target, CTAG elements are torsionally rigid relative to generic B-DNA sequences.

The twist flexibility of the Con1–Con3 sequences and the binding affinity and binding cooperativity of these

sequences show similar trends. The torsionally flexible Con1 target has the lowest binding cooperativity, the intermediate dimer species is long-lived and stable enough to show up as a separate entity on EMSA gels, and the affinity of the tetrameric complex is the highest of the series. The relatively more rigid Con2 and Con3 targets show only tetramer bands of lower relative affinity. We suggest that it is the flexible nature of the Con1 target that reduces its cooperativity of interaction and allows the formation of a long-lived and stable dimer intermediate, on the way to the functional tetramer species. The facile winding/unwinding motion of the CATG motif allow the stabilization of inter-subunit interactions within p53DBD, such that binding of only one dimer to DNA is stable, the cooperativity is thus low and the binding affinity is relatively high, for both the tetramer and the dimer (Table 1). This is not the case for the more torsionally constrained CAAG (Con3) and the CTAG (Con2) containing targets.

The significance of torsional flexibility in p53/DNA interactions can be clearly visualized by calculating the expected free energy difference of twisting p53 binding sites by the twist angle observed in crystal structures. In the GGG structure (Con4 in Table 2, the most torsionally flexible target), the difference between the A-T (24.1°) and the T-G (43.8°) steps is 19.7° in twist angle (12). Similar differences in the center CATG core have been observed in other p53/DNA complexes with a CATG center (63,64). The free energy difference for this amount of twist change is 2.43×10^{-13} erg or six times the thermal energy (k_BT) at 21°C (the temperature at which the torsional force constant was measured). For the Con2 target, the free energy difference for the same twist angle change is 6.64×10^{-13} erg, or nine times the thermal energy at 21°C. Thus, there is a 50% difference in the energetic cost of twisting these two targets.

It was previously suggested (17,44) that DNA flexibility of p53 REs containing the CATG motif is an important factor in the enhanced binding affinity of such sites, but these discussions do not differentiate between axial (bending) flexibility and torsional (twist) flexibility. We showed that there is '*no axial flexibility*' intrinsic to the studied p53 targets, only '*torsional flexibility*'. Nagaich *et al*. (65) observed, by gel studies, that a sequence identical to the AGG target (12) is bent in solution in its free state. We did not observe any static bending, or any bendability of the sequences studies here and also not when the AGG (Con6, Table 2) target was studied by cyclization kinetics. Our study is the first study to experimentally determine the global structure and mechanical properties of p53 REs by a sensitive and rigorous technique, carried out completely in solution, which does not rely on external calibrators and is based on a complete theoretical basis (66).

In the recent crystal structure determination of a 20-bp duplex incorporating two contiguous decamers bound to p53DBD, each DNA half-site is only slightly bent, and the combined two half-sites are straight (67). Bending of the magnitude displayed in this structure (as well as other crystal structures of p53DBD/DNA complexes, refs. 12,13,63,64,68) is accessible to generic B-DNA molecules that are not particularly axially flexible (the free energy of ~20° or lower overall bends /10 bp is below thermal energy at 25°C, ref. 54). Thus, the energetic penalty cost for formation of complexes with such bend magnitude is negligible. This is in line with our observations of an average axial flexibility in the three target sites examined here, regardless of their binding affinity. On the other hand, twist flexibility of p53 DNA targets may be functionally important. In the crystal structure determination of two contiguous decamers bound to p53DBD (67), the base pairing at the central A-T doublet shows the Hoogsteen geometry. Further characterization, by the Shakked group (67), of the mouse p53DBD tetramer covalently linked to a DNA duplex (64), shows that a large fraction of the A-T central doublet is in the Hoogsteen geometry also in this structure. The ability of CATG containing DNA sequences, in complex with p53DBD, to adopt both the Watson–Crick as well as the Hoogsteen geometry is an indication of their large torsional flexibility, because the flip from Watson–Crick to Hoogsteen geometry and vice versa should involve winding and unwinding of the double helix.

Creating a torsional swivel in Con3 reduces its binding cooperativity and stabilizes a bound dimer

To further corroborate our suggestion that torsional flexibility is responsible for the difference in binding affinity and cooperativity between sites differing in the non-contacted step of the CWWG region, we introduced a torsional swivel into the Con3 target (nicked Con3, Table 1) by designing it as an intramolecular dumbbell, containing two hairpin loops. The 5′ and 3′ ends meet at the middle of the 5′ half-site, and thus there is a nick in the 5′ half-site sequence between the C-A and A-G steps, which renders the nicked Con3 target highly torsionally flexible (as shown in other protein–DNA systems; refs. 31,32). The EMSA pattern for the nicked Con3 target and p53DBD (Figure 5) showed two bound bands, albeit less sharply defined than those of Con1. Quantitative analysis (Figure 3D and Table 1) was again carried out using a two binding site model. The analysis had now to be performed in terms of the macroscopic constants, since the two half-sites are not identical anymore. However, we can estimate the intrinsic binding constant of the nicked half-site (k_2) using the relationship $K_{a1} = k_1 + k_2$, assuming that we can take the intrinsic binding constant of the intact half-site (k_1) from measurements of intact Con3. Such analysis showed that the nicked Con3 half-site [600 (100) nM, Table 1] have ~20-fold higher affinity compared to the estimated K_d of the dimer from the intact Con3 half-site. The cooperativity constant can be estimated from the expression of K_{a2} and the known values for k_1 and k_2, and it value [9.0 (0.6)] showed that the binding cooperativity to the nicked Con3 binding site is lower than that to the flexible Con1 site. DNA with a nick in the backbone (and with a 3′-end phosphate) was shown by Zhang and Crothers (32) to have twist fluctuations of 6.8 (1.2)°, significantly more flexible than Con1. Such high twist flexibility allows the monomers within each dimer to re-adjust their relative

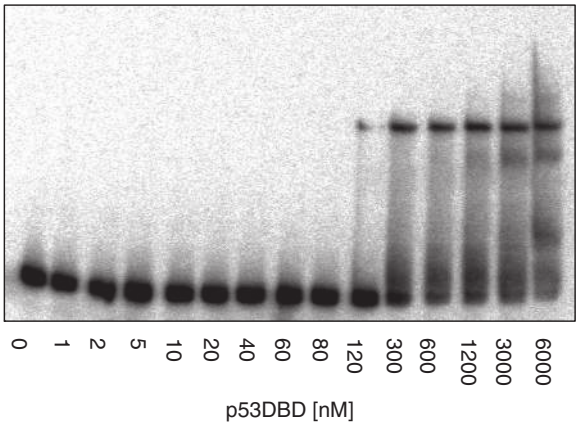

Figure 5. Binding affinity measurements by EMSA of p53DBD binding to the Con3 target with a nick in the center of the 5′-half-site (as shown in Table 1). This DNA target was synthesized as an intramolecular dumbbell construct with two hairpin loops. For other details, see Figure 1.

conformation at low energetic cost, and thus they form stable and long-lived dimers, leading to low cooperativity of interaction of the nicked Con3 with p53DBD. This extends the trend observed with the Con1–Con3 series of inverse relationship between twist flexibility and cooperativity–high twist flexibility and low cooperativity of interaction and vice versa. However, here the trend does not include high affinity of tetramers of p53DBD binding to targets with high twist flexibility. The binding affinity of the tetramer complex to nicked Con3 was significantly reduced (Table 1) relative to that of intact Con3, probably due to lose of contacts to the DNA backbone (12).

Binding of p53DBD to p53 targets with spacers between half-sites

In the p53 consensus the two half-sites can be separated by up to 13 bp (4). More recent studies show, however, that spacer sequences of more than a few nucleotides decrease p53 responsiveness from these sites (11,20), and attenuates p53 binding affinity (44). We asked whether the differential effects of the non-contacted WW step shown above would differently affect binding, when spacer sequences are introduced into the Con1 versus the Con2 targets. For the Con1 target with spacers between half-sites the observed gel pattern (Figure 6A and B) was again of two bound complexes, dimers and tetramers of p53DBD, as previously observed by Kitayner *et al.* (12). Comparing the binding pattern of Con1, Con1 and 2-bp spacer, and Con1 and 4-bp spacer side-by-side on the same gel (Supplementary Figure S5) showed that the dimeric species migrated to the same distance on the gel in all complexes with these targets. The tetrameric species migrated to decreasing distances on the gel as a function of the spacer length. This may be due to differences in twisting of the DNA in the complexes. Quantitative analysis of the binding affinity of p53DBD to these sites (Figure 3E and F and Table 1) showed that the dimeric species bound with slightly reduced K_d to that observed in the Con1 target [442 (20) nM and 581 (46) nM for the insertion of 2- and 4-bp spacer respectively, Table 1]. Significant reduction in binding affinity relative to that in Con1 was observed for the tetrameric species [435 (32) nM and 1.02 (0.06) μM for the sites with 2- and 4-bp spacers respectively, Table 1], corresponding to reduced protein–protein interactions in the inter-dimer interface, in comparison to protein–protein contacts in the complex with contiguous DNA site (67). The cooperativity of interaction is reduced from that observed for Con1 to 1.1(1) with 2-bp spacer and 0.34 (0.06) with 4-bp spacer (Table 1). Altogether, the cooperativity differences between p53 target sites spanned five orders of magnitude, as a function of binding site sequence and spacers. No significant binding, of either binding stoichiometry, can be observed to the Con2 targets with spacer sequences (Figure 6C and D). Analysis (Figure 3G and H and Table 1) showed that the binding affinity for both species is in the micromolar range.

Binding of p53DBD to p53 half-sites

Binding affinity of the dimeric species can be affected by gel instabilities from the tetrameric band above it. To avoid this, and to explore whether p53DBD binds half-sites as dimers or tetramers, we constructed target sites comprising only one specific decamer, embedded in the center of a hairpin of the same length as the other sites, such that there are no surrounding nonspecific decameric half-sites. EMSA pattern with the Con1 half-site (Con1 HS, Figure 7A) had one bound species, identified by a Job plot analysis (Supplementary Figure S6) as a dimer. Analysis of binding affinity by a one-site model (Figure 3I) yielded a K_d of 305 (24) nM, which is similar to that of the dimeric complexes with Con1. Again, no appreciable binding was observed to Con2 half-site (Con2 HS, Figure 7B). Binding affinity to Con2 HS is again in the micromolar range (Figure 3J and Table 1).

Statistical analysis of validated p53 half-sites grouped by the central CNNG motif

We have measured in this study the flexibility of six defined p53 consensus targets, with variations in the CWWG motif at their center, and noted a significant difference in the observed torsional flexibility of the A-T containing targets from that observed in the T-A or the A-A targets. Other central dinucleotide steps are found in natural p53 REs (within CNNG motifs), and they are imbedded within different flanking contexts, which have a consensus of RRR (and YYY), but from which most p53 REs deviate, in at least one position (42,44). We wanted to assess the centrality of the structural properties of the core CNNG motif in determining the overall intrinsic flexibility of p53 RE half-sites (that is along the entire decameric half-site). Thus, we asked whether we can group all available p53 RE half-sites, based on the identity of the central tetranucleotide, and whether such clustering will result in groups that are significantly distinct from each other, based on their structural parameters. In order to carry out such analysis, we assumed that we can represent DNA sequences

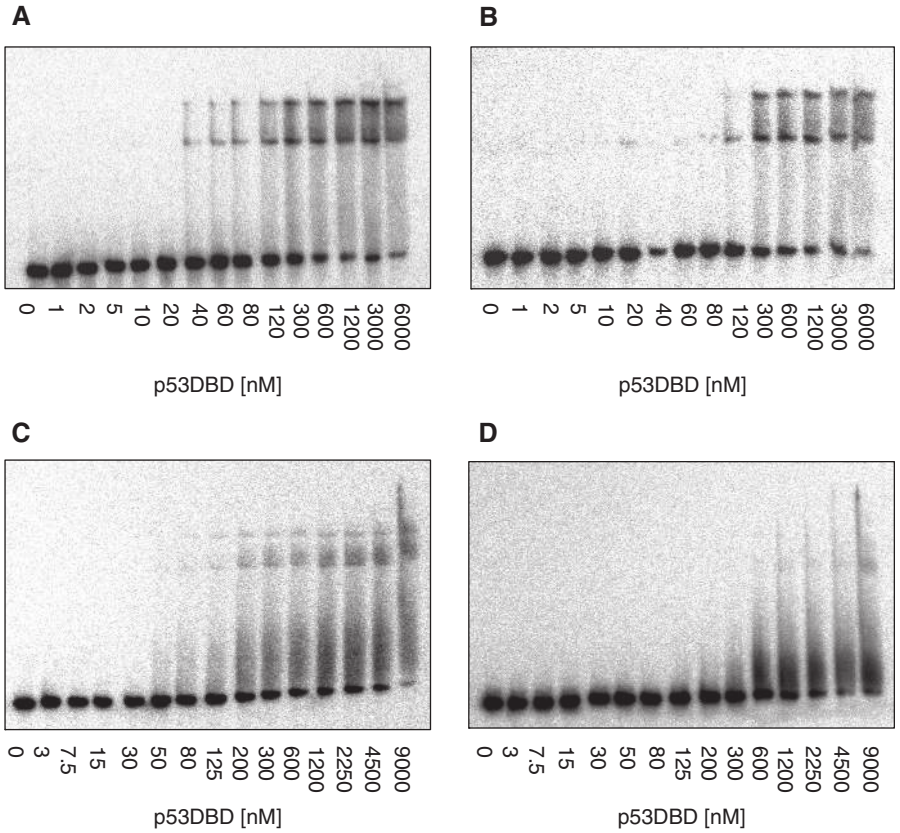

Figure 6. Binding affinity measurements by EMSA of p53DBD binding to REs with spacers between half-sites. (**A**) Con1 with 2-bp spacer. (**B**) Con1 with 4-bp spacer. (**C**) Con2 with 2-bp spacer. (**D**) con2 with 4-bp spacer. For details, see Figure 1.

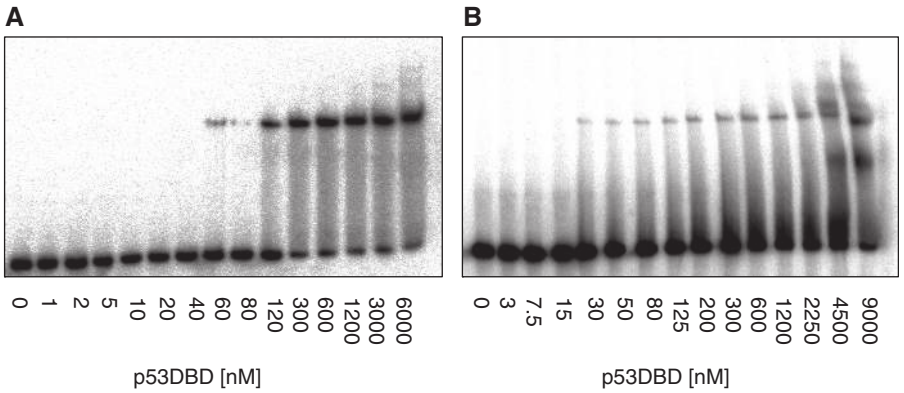

Figure 7. Binding affinity measurements by EMSA of p53DBD binding to half-site REs. (**A**) Con1HS. (**B**) Con2HS. For details, see Figure 1. The band below the bound band in (B) (which is a complex of p53DBD dimer to con2HS) may be a p53DBD monomer bound to con2HS.

based on nearest-neighbor interactions only, so that we can carry out calculations on the structural deformability of DNA sequences from knowledge of the deformability of all DNA doublets. Olson *et al.* (41) have studied the sequence-dependent deformability of DNA doublets, based on their conformation in protein–DNA complexes. This data set was the only available dinucleotide properties dataset that when we used it to calculate the torsional flexibility of the six p53 binding sites for which we have cyclization kinetics data, we got a good-enough correspondence between the dispersion values of dinucleotide steps around their mean value and our experimental measurements ($\rho = 0.971$, $P = 0.04$) to suggest that these dispersion values can be used as a measure for the intrinsic sequence-dependent flexibility of DNA base-pair steps.

DNA structural parameters that show the largest variability, as a function of base-pair step identity, are twist, roll and slide (41,69,70). We therefore calculated the mean twist, roll and slide flexibility for each known p53 RE half-site (42), using the dispersion values from Olson *et al.* (41), and then calculated the mean of the mean for sequences grouped by the central tetranucleotide. We

included in this analysis only p53 REs that have decameric half-sites and that contain a central CNNG core. The results (Supplementary Table S1) showed that sequences with a CATG center have the highest torsional flexibility, slide flexibility and roll flexibility, whereas sequences with a CTAG center have the lowest flexibility in these parameters, relative to CATG or CAAG, even though now the sequences have various sequence motifs flanking a specific central tetranucleotide core. We carried out statistical tests to assess the significance of these results (Supplementary Table S2), which showed that the differences between CATG and either CAAG or CTAG groups are highly significant (*P*-values are 4.0E-10 and lower), in either rotational twist flexibility or translational slide flexibility. Overall, the differences between the groups with respect to changes in the roll parameter are of lower significance. Many other significant differences can be noted, especially between CATG and other groups, or CTAG and other groups, because these two groups are the two extreme ends of values of flexibility parameters. Even if we multiply the *P*-values by 45, to account for multiple comparisons (15 comparisons and by three parameters, ref. 43) many significant differences remain, especially between CATG and other groups, and CTAG and other groups. Changes in twist, slide and roll are not independent of each other (41,70,71); however, as the differences between the groups are so significant, there is no need to carry out a multivariate analysis to test for significant clustering patterns using twist, slide and roll dispersion together.

Function from p53 half-sites follows their binding and structural characteristics

It is now established that p53 can function also from p53 half-sites. Menendez *et al*. (72) showed that a p53 consensus half-site generated by a C to T SNP in the flt-1 promoter can support ~25% of the transactivation level of the p21-5′ RE. Combined with a nearby estrogen receptor RE, and upon treatment with estradiol, the transactivation level increases 4-fold, to that from the potent p21-5′ RE (73). That p53 can transactivate from p53 half-sites was also established from half-site RE found in the RAP80 promoter (74), where only slight reduction is observed relative to the full RE (the full RE contains a 4-bp spacer). These results expand the universe of potential p53 RE and with it the ability to fine tune p53 regulated genes. A clear trend can be established between the identity of the CWWG motif and transactivation from p53 half-sites (20). A sequence identical to Con1HS (with a CATG center) showed the highest transactivation level of all CWWG half-site variants, followed by Con3HS (with CAAG, 5-fold reduction in transcription level), whereas Con2HS (with a CTAG center) hardly showed any transactivation ability (20). This follows our binding affinity measurements as well as the torsional flexibility of the CWWG sites studied here. Based on our results we interpret these observations as resulting from the inability of p53 to bind CTAG containing half-sites, which is due to the relative torsional rigidity of such sequences.

Cooperative binding by p53DBD—implications for functional binding by full-length p53 and by p53 isoforms

Here, we studied the binding characteristics of p53DBD to several consensus target sites. This is not the functional form of p53 *in vivo*. However, it is now known that the *p53* gene encodes at least ten different p53 protein isoforms as a result of alternative splicing (75–78). Some variants lack part of the N-terminal region (the TA domain), whereas other variants lack the parts of the tetramerization domain and/or the extreme C-terminal regulatory domain (78). It has been suggested that p53 isoforms may modulate wt p53 (the canonical form of p53) activity by modulating DNA binding, by the formation of hetero-oligomers, and/or by sequestering p53 in the cytoplasm. Alternatively, p53 isoforms may have autonomous specialized functions (78). This may be isoform dependent and/or cell-type specific (77,78). Furthermore, p53 isoforms arise most commonly because of splice-site mutations, which may lead to exon skipping, or the creation of new splice sites (79,80). Although at this stage the observations on p53 isoforms, in normal and cancerous cells, are sometimes conflicting (discussed in refs. 78 and 81–83), advancing our detailed understanding of the ability of various p53 truncation constructs to bind various p53 target sites is important for cancer diagnosis and treatment.

We showed in this study that there are five order of magnitude changes of cooperative binding of p53DBD to specific targets as a function of changes in consensus sequences. Whenever the cooperativity constant is above ~1000 no intermediate species are observed (37). Indeed, for complexes of p53DBD with the Con2 and Con3 targets no dimer bands are observed. Nonetheless, there is a significant change in cooperative interaction between these two sites. The binding of full-length p53 to DNA was suggested to be as cooperative (or more) than the binding of p53DBD to DNA (24). We suggest that binding of full-length p53 to DNA may show similar cooperativity changes as a function of DNA base sequence, even though it may bind to it REs only as a tetramer, because of higher cooperativity of interaction. Further studies will provide information on the effect of domains outside the DBD on sequence-dependent binding cooperativity of p53 to its REs.

SUPPLEMENTARY DATA

Supplementary Data are available at NAR Online.

ACKNOWLEDGEMENT

We thank Zippi Shakked for purified p53DBD and p53TD, for critical reading of the manuscript, and for many helpful discussions. We thank Yongli Zhang and Don Crothers for initiating us into the cyclization kinetics method. We thank Mike Fried for bringing into our attention the continuous variation method for stoichiometry determination. We thank Mike Resnick for critical reading of an initial version of this manuscript. We thank Lev Greenberg for help with the statistical analysis.

FUNDING

The Israel Science Foundation (grant No.104405); Israel Cancer Research Fund (grant No. 800005); German-Israel Foundation (grant No. 890007). Funding for open access charge: Israel Cancer Research Fund.

Conflict of interest statement. None declared.

REFERENCES

1. Vogelstein,B., Lane,D. and Levine,A.J. (2000) Surfing the p53 network. *Nature*, **408**, 307–310.
2. Vousden,K.H. and Lu,X. (2002) Live or let die: the cell's response to p53. *Nat. Rev. Cancer*, **2**, 594–604.
3. Oren,M. (2003) Decision making by p53: life, death and cancer. *Cell Death Differ.*, **10**, 431–442.
4. El-Deiry,W.S., Kern,S.E., Pietenpol,J.A., Kinzler,K.W. and Vogelstein,B. (1992) Definition of a consensus binding site for p53. *Nature Gen.*, **1**, 45–49.
5. Funk,W.D., Pak,D.T., Karas,R.H., Wright,W.E. and Shay,J.W. (1992) A transcriptionally active DNA-binding site for human p53 protein complexes. *Mol. Cell Biol.*, **12**, 2866–2871.
6. Vousden,K.H. and Lane,D.P. (2007) p53 in health and disease. *Nat. Rev. Mol. Cell. Biol.*, **8**, 275–283.
7. Vousden,K.H. and Prives,C. (2009) Blinded by the light: the growing complexity of p53. *Cell*, **137**, 413–431.
8. Laptenko,O. and Prives,C. (2006) Transcriptional regulation by p53: one protein, many possibilities. *Cell Death Differ.*, **13**, 951–961.
9. Hupp,T.R. (1999) Regulation of p53 protein function through alterations in protein-folding pathways. *Cell. Mol. Life Sci.*, **55**, 88–95.
10. Weisz,L., Oren,M. and Rotter,V. (2007) Transcription regulation by mutant p53. *Oncogene*, **26**, 2202–2211.
11. Tokino,T., Thiagalingam,S., el-Deiry,W.S., Waldman,T., Kinzler,K.W. and Vogelstein,B. (1994) p53 tagged sites from human genomic DNA. *Hum. Mol. Genet.*, **3**, 1537–1542.
12. Kitayner,M., Rozenberg,H., Kessler,N., Rabinovich,D., Shaulov,L., Haran,T.E. and Shakked,Z. (2006) Structural basis of DNA recognition by p53 tetramers. *Mol. Cell*, **22**, 741–753.
13. Cho,Y., Gorina,S., Jeffrey,P.D. and Pavletich,N.P. (1994) Crystal structure of a p53 tumor suppressor–DNA complex: understanding tumorigenic mutations. *Science*, **265**, 346–355.
14. Qian,H., Wang,T., Naumovski,L., Lopez,C.D. and Brachmann,R.K. (2002) Groups of p53 target genes involved in specific p53 downstream effects cluster into different classes of DNA binding sites. *Oncogene*, **21**, 7901–7911.
15. Hoh,J., Jin,S., Parrado,T., Edington,J., Levine,A.J. and Ott,J. (2002) The p53MH algorithm and its application in detecting p53-responsive genes. *Proc. Natl Acad. Sci. USA*, **99**, 8467–8472.
16. Wei,C.L., Wu,Q., Vega,V.B., Chiu,K.P., Ng,P., Zhang,T., Shahab,A., Yong,H.C., Fu,Y., Weng,Z. *et al.* (2006) A global map of p53 transcription-factor binding sites in the human genome. *Cell*, **124**, 207–219.
17. Weinberg,R.L., Veprintsev,D.B., Bycroft,M. and Fersht,A.R. (2005) Comparative binding of p53 to its promoter and DNA recognition elements. *J. Mol. Biol.*, **348**, 589–596.
18. Inga,A., Storici,F., Darden,T.A. and Resnick,M.A. (2002) Differential transactivation by the p53 transcription factor is highly dependent on p53 level and promoter target sequence. *Mol. Cell. Biol.*, **22**, 8612–8625.
19. Wang,B., Xiao,Z. and Ren,E.C. (2009) Redefining the p53 response element. *Proc. Natl Acad. Sci. USA*, **106**, 14373–14378.
20. Jordan,J.J., Menendez,D., Inga,A., Nourredine,M., Bell,D. and Resnick,M.A. (2008) Noncanonical DNA motifs as transactivation targets by wild type and mutant p53. *PLoS Genet.*, **4**, e1000104.
21. Wang,Y., Schwedes,J.F., Parks,D., Mann,K. and Tegtmeyer,P. (1995) Interaction of p53 with its consensus DNA-binding site. *Mol. Cell. Biol.*, **15**, 2157–2165.
22. Balagurumoorthy,P., Sakamoto,H., Lewis,M.S., Zambrano,N., Clore,G.M., Gronenborn,A.M., Appella,E. and Harrington,R.E. (1995) Four p53 DNA-binding domain peptides bind natural p53-response elements and bend the DNA. *Proc. Natl Acad. Sci. USA*, **92**, 8591–8595.
23. McLure,K.G. and Lee,P.W.K. (1998) How p53 binds DNA as a tetramer. *EMBO J.*, **17**, 3342–3350.
24. Weinberg,R.L., Veprintsev,D.B. and Fersht,A.R. (2004) Cooperative binding of tetrameric p53 to DNA. *J. Mol. Biol.*, **341**, 1145–1159.
25. Dehner,A., Klein,C., Hansen,S., Muller,L., Buchner,J., Schwaiger,M. and Kessler,H. (2005) Cooperative binding of p53 to DNA: regulation by protein–protein interactions through a double salt bridge. *Angew. Chem. Int. Ed. Engl.*, **44**, 5247–5251.
26. Klein,C., Planker,E., Diercks,T., Kessler,H., Kunkele,K.P., Lang,K., Hansen,S. and Schwaiger,M. (2001) NMR spectroscopy reveals the solution dimerization interface of p53 core domains bound to their consensus DNA. *J. Biol. Chem.*, **276**, 49020–49027.
27. Rippin,T.M., Freund,S.M., Veprintsev,D.B. and Fersht,A.R. (2002) Recognition of DNA by p53 core domain and location of intermolecular contacts of cooperative binding. *J. Mol. Biol.*, **319**, 351–358.
28. Veprintsev,D.B., Freund,S.M., Andreeva,A., Rutledge,S.E., Tidow,H., Canadillas,J.M., Blair,C.M. and Fersht,A.R. (2006) Core domain interactions in full-length p53 in solution. *Proc. Natl Acad. Sci. USA*, **103**, 2115–2119.
29. Gasteiger,E., Hoogland,C., Gattiker,A., Duvaud,S., Wilkins,M.R., Appel,R.D. and Bairoch,A. (2005) In Walker,J.M. (ed.), *The Proteomics Protocols Handbook*. Humana Press Inc., Totowa, NJ, pp. 571–607.
30. Bareket-Samish,A., Cohen,I. and Haran,T.E. (2000) Signals for TBP/TATA box recognition. *J. Mol. Biol.*, **299**, 965–977.
31. Hines,C.S., Meghoo,C., Shetty,S., Biburger,M., Brenowitz,M. and Hegde,R.S. (1998) DNA structure and flexibility in the sequence-specific binding of papillomavirus E2 proteins. *J. Mol. Biol.*, **276**, 809–818.
32. Zhang,Y. and Crothers,D.M. (2003) High-throughput approach for detection of DNA bending and flexibility based on cyclization. *Proc. Natl Acad. Sci. USA*, **100**, 3161–3166.
33. Huang,C.Y. (1985) Determination of binding stoichiometry by the continuous variation method: the Job plot. *Methods Enzymol.*, **87**, 509–525.
34. Bareket-Samish,A., Cohen,I. and Haran,T.E. (1997) Repressor assembly at *trp* binding sites is dependent on the identity of the intervening dinucleotide between the binding half sites. *J. Mol. Biol.*, **267**, 103117.
35. Eisenberg,D.S. and Crothers,D.M. (1979) *Physical Chemistry with Applications in the Life Sciences*, Benjamin/Cummings Pub. Comp., Menlo Park, CA.
36. Fried,M. and Crothers,D.M. (1981) Equilibria and kinetics of *lac* repressor–operator interactions by polyacrylamide gel electrophoresis. *Nucleic Acids Res.*, **9**, 6505–6525.
37. Senear,D.F. and Brenowitz,M. (1991) Determination of binding constants for cooperative site-specific protein–DNA interactions using the gel mobility-shift assay. *J. Biol. Chem.*, **266**, 13661–13671.
38. Jacobson,H. and Stockmayer,W.H. (1950) Intramolecular reaction in polycondensations. 1. The theory of linear systems. *J. Chem. Phys.*, **18**, 1600–1606.
39. Shore,D., Langowski,J. and Baldwin,R.L. (1981) DNA flexibility studied by covalent closure of short fragments into circles. *Proc. Natl Acad. Sci. USA*, **78**, 4833–4837.
40. Zhang,Y. and Crothers,D.M. (2003) Statistical mechanics of sequence-dependent circular DNA and its application for DNA cyclization. *Biophys. J.*, **84**, 136–153.
41. Olson,W.K., Gorin,A.A., Lu,X.J., Hock,L.M. and Zhurkin,V.B. (1998) DNA sequence-dependent deformability deduced from protein–DNA crystal complexes. *Proc. Natl Acad. Sci. USA*, **95**, 11163–11168.
42. Menendez,D., Inga,A. and Resnick,M.A. (2009) The expanding universe of p53 targets. *Nat. Rev. Cancer.*, **9**, 724–737.
43. Moore,D.S. and McCabe,G.P. (1989) *Introduction to the Practice of Statistics*. W. H. Freeman and Company, New York.

44. Riley,T., Sontag,E., Chen,P. and Levine,A. (2008) Transcriptional control of human p53-regulated genes. *Nat. Rev. Mol. Cell Biol.*, **9**, 402–412.
45. Fried,M.G. and Daugherty,M.A. (1998) Electrophoretic analysis of multiple protein–DNA interactions. *Electrophoresis*, **19**, 1247–1253.
46. Adams,C.A. and Fried,M.G. (2007) In. In Schuck,P. (ed.), *Protein Interactions: Biophysical Approaches for the Study of Complex Reversible Systems*. Academic Press, New York, pp. 417–446.
47. Hope,I.A. and Struhl,K. (1987) GCN4, a eukaryotic transcriptional activator protein, binds as a dimer to target DNA. *EMBO J.*, **6**, 2781–2784.
48. Cain,C., Miller,S., Ahn,J. and Prives,C. (2000) The N terminus of p53 regulates its dissociation from DNA. *J. Biol. Chem.*, **275**, 39944–39953.
49. Faiger,H., Ivanchenko,M., Cohen,I. and Haran,T.E. (2006) TBP flanking sequences: asymmetry of binding, long-range effects and consensus sequences. *Nucleic Acids Res.*, **34**, 104–119.
50. Faiger,H., Ivanchenko,M. and Haran,T.E. (2007) Nearest-neighbor non-additivity versus long-range non-additivity in TATA-box structure and its implications for TBP-binding mechanism. *Nucleic Acids Res.*, **35**, 4409–4419.
51. Carey,J. (1988) Gel retardation at low pH resolves *trp* repressor–DNA complexes for quantitative study. *Proc. Natl Acad. Sci. USA*, **85**, 975–979.
52. Fried,M.G. (1989) Measurement of protein–DNA interaction parameters by electrophoresis mobility shift assay. *Electrophoresis*, **10**, 366–376.
53. Cann,J.R. (1989) Phenomenological theory of gel electrophoresis of protein–nucleic acid complexes. *J. Biol. Chem.*, **264**, 17032–17040.
54. Bloomfield,V.A., Crothers,D.M. and Tinoco,I.J. (2000) *Nucleic Acids: Structures, Properties, and Functions*. University Science Books, Sausalito.
55. Dickerson,R.E. (1998) DNA bending: the prevalence of kinkiness and the virtues of normality. *Nucleic Acids Res.*, **26**, 1906–1926.
56. Zhang,Y., Xi,Z., Hegde,R.S., Shakked,Z. and Crothers,D.M. (2004) Predicting indirect readout effects in protein–DNA interactions. *Proc. Natl Acad. Sci. USA*, **101**, 8337–8341.
57. Fujimoto,B.S. and Schurr,J.M. (1990) Dependence of the torsional rigidity of DNA on base composition. *Nature*, **344**, 175–177.
58. Chen,H.H., Rau,D.C. and Charney,E. (1985) The flexibility of alternating dA-dT sequences. *J. Biomol. Struct. Dyn.*, **2**, 709–719.
59. Gorin,A.A., Zhurkin,V.B. and Olson,W.K. (1995) B-DNA twisting correlates with base-pair morphology. *J. Mol. Biol.*, **247**, 34–48.
60. Dlakic,M. and Harrington,R.E. (1995) Bending and torsional flexibility of G/C-rich sequences as determined by cyclization assays. *J. Biol. Chem.*, **270**, 29945–29952.
61. Travers,A.A. and Klug,A. (1990) In. In Cozzarelli,N.R. and Wang,J.C. (eds), *DNA Topology and Its Biological Effects*. Cold Spring Harbor Press, Cold Spring Harbor, pp. 57–106.
62. Widom,J. (2001) Role of DNA sequence in nucleosome stability and dynamics. *Q. Rev. Biophys.*, **34**, 269–324.
63. Ho,W.C., Fitzgerald,M.X. and Marmorstein,R. (2006) Structure of the p53 core domain dimer bound to DNA. *J. Biol. Chem.*, **281**, 20494–20502.
64. Malecka,K.A., Ho,W.C. and Marmorstein,R. (2009) Crystal structure of a p53 core tetramer bound to DNA. *Oncogene*, **28**, 325–333.
65. Nagaich,A., Zhurkin,V.B., Durrel,S.R., Jernigan,R.L., Appella,E. and Harrington,R.E. (1999) p53-induced DNA bending and twisting:p53 tetramer binds on the outer side of a DNA loop and increases DNA twisting. *Proc. Natl Acad. Sci. USA*, **96**, 1875–1880.
66. Crothers,D.M., Drak,J., Kahn,J.D. and Levene,S.D. (1992) DNA bending, flexibility, and helical repeat by cyclization kinetics. *Methods Enzymol.*, **212**, 3–29.
67. Kitayner,M., Rozenberg,H., Rohs,R., Suad,O., Rabinovich,D., Honig,B. and Shakked,Z. (2010) Diversity in DNA recognition by p53 revealed by crystal structures with Hoogsteen base pairs. *Nat. Struct. Mol. Biol.*, **17**, 423–429.
68. Chen,Y., Dey,R. and Chen,L. (2010) Crystal structure of the p53 core domain bound to a full consensus site as a self-assembled tetramer. *Structure*, **18**, 246–256.
69. Shakked,Z. and Rabinovich,D. (1986) The effect of the base sequence on the fine structure of the DNA double helix. *Prog. Biophys. Mol. Biol.*, **47**, 159–195.
70. El Hassan,M. and Calladine,C.R. (1997) Conformational characteristics of DNA: empirical classifications and a hypothesis for the conformational behaviour of dinucleotide steps. *Phil. Trans. Roy. Soc. Lond.*, **A 355**, 43–100.
71. Dickerson,R.E. (1999) In. In Neidle,S. (ed.), *Oxford Handbook of Nucleic Acid Structure*. Oxford University Press, New York, pp. 145–197.
72. Menendez,D., Krysiak,O., Inga,A., Krysiak,B., Resnick,M.A. and Schonfelder,G. (2006) A SNP in the flt-1 promoter integrates the VEGF system into the p53 transcriptional network. *Proc. Natl Acad. Sci. USA*, **103**, 1406–1411.
73. Menendez,D., Inga,A., Snipe,J., Krysiak,O., Schonfelder,G. and Resnick,M.A. (2007) A single-nucleotide polymorphism in a half-binding site creates p53 and estrogen receptor control of vascular endothelial growth factor receptor 1. *Mol. Cell Biol.*, **27**, 2590–2600.
74. Yan,J., Menendez,D., Yang,X.P., Resnick,M.A. and Jetten,A.M. (2009) A regulatory loop composed of RAP80-HDM2-p53 provides RAP80-enhanced p53 degradation by HDM2 in response to DNA damage. *J. Biol. Chem.*, **284**, 19280–19289.
75. Bourdon,J.C., Fernandes,K., Murray-Zmijewski,F., Liu,G., Diot,A., Xirodimas,D.P., Saville,M.K. and Lane,D.P. (2005) p53 isoforms can regulate p53 transcriptional activity. *Genes Dev.*, **19**, 2122–2137.
76. Rohaly,G., Chemnitz,J., Dehde,S., Nunez,A.M., Heukeshoven,J., Deppert,W. and Dornreiter,I. (2005) A novel human p53 isoform is an essential element of the ATR-intra-S phase checkpoint. *Cell*, **122**, 21–32.
77. Khoury,M.P. and Bourdon,J.C. (2010) The isoforms of the p53 protein. *Cold Spring Harb. Perspect. Biol.*, **2**, a000927.
78. Marcel,V. and Hainaut,P. (2009) p53 isoforms - a conspiracy to kidnap p53 tumor suppressor activity? *Cell. Mol. Life Sci.*, **66**, 391–406.
79. Holmila,R., Fouquet,C., Cadranel,J., Zalcman,G. and Soussi,T. (2003) Splice mutations in the p53 gene: case report and review of the literature. *Hum. Mutat.*, **21**, 101–102.
80. Hofstetter,G., Berger,A., Fiegl,H., Slade,N., Zoric,A., Holzer,B., Schuster,E., Mobus,V.J., Reimer,D., Daxenbichler,G. *et al.* (2010) Alternative splicing of p53 and p73: the novel p53 splice variant p53delta is an independent prognostic marker in ovarian cancer. *Oncogene*, **29**, 1997–2004.
81. Deppert,W. (2009) Alternatively spliced p53 isoforms: alternative views or alternative functions? *Cell Cycle*, **8**, 1645.
82. Bourdon,J.C. (2007) p53 and its isoforms in cancer. *Br. J. Cancer*, **97**, 277–282.
83. Machado-Silva,A., Perrier,S. and Bourdon,J.C. (2010) p53 family members in cancer diagnosis and treatment. *Semin. Cancer Biol.*, **20**, 57–62.